Road noise sensitivity analysis with respect to suspension geometry

Fumihiko KOSAKA[1]; Hiroaki MIZUNO[2]; Tsuyoshi INOUE[3]; Kentaro TAKAGI[4]

[1, 2] MITSUBISHI MOTORS CORPORATION, Japan

[3, 4] Nagoya University, Japan

ABSTRACT

In the vehicle development, the importance of reducing road noise is increasing because of the increasing popularity of quiet electric vehicle. The suspension plays an important role on the mechanism of the structure born road noise. As the countermeasure for reducing road noise, low stiffness suspension bush is often used from the point of view of vibration insulation. However, in general, to use the low stiffness suspension bush makes the driving stability worse. From such reason, it has been difficult to achieve the compatibility between NVH and driving stability at high quality. Therefore, the other ways are required for reducing the road noise. As one of the ways, the road noise reduction by the suspension geometry is presented in this paper. In order to find the suspension geometry which reduces the road noise, the sensitivity analysis is used. For the sensitivity analysis with respect to the position of the suspension arm connecting points, the suspension model is simplified. The arms are modeled as rigid links whereas the vehicle body, tire and shock absorber are modeled as a modal model. The suspension geometry which reduces the road noise is obtained with the sensitivity analysis.

Keywords: Suspension, Sensitivity, Road noise I-INCE Classification of Subjects Number(s): 46, 76

1. INTRODUCTION

Recently, the importance of reducing road noise of the vehicle is increasing because of the increase popularity of quiet electric vehicle. On the mechanism of structure born road noise, the suspension plays an important role. As a typical countermeasure for reducing road noise in the vehicle development, low stiffness bush are often used from the point of view of vibration insulation. However, in general, this makes the handling stability worse. The suspension design which achieves the compatibility between NVH and handling stability at high quality is required.

In spite of such a circumstance, there are not so many literatures written about the road noise reduction by the suspension. This would be because of the difficulties in controlling the vibration behavior of the suspension. The vibration energy transmits through the multiple connection points at which the suspension is connected to the vehicle body. When one of the connection points highly contributes to the energy transmission, it may be thought that reducing the vibration of this point will reduce the road nose. However, some countermeasures for this point might increase the vibrations at the other connection points because the local countermeasure may affect the global suspension vibration behavior. Thus, the countermeasures that consider the trade-off among the vibrations of the each connection points are required.

The countermeasures for reducing the road noise would be about the suspension bushes or the suspension geometry. In general, the suspension bushes could be modified at the later stage of the vehicle development, however, the suspension geometry is fixed at the early stage and could not be able to be modified at the later stage. Therefore, in this paper, for increasing the possibility of the compatibility at high quality, the focus is given to the road noise reduction by the suspension geometry.

[1] fumihiko.kosaka@mitsubishi-motors.com
[2] hiroaki1.mizuno@mitsubishi-motors.com
[3] inoue@nuem.nagoya-u.ac.jp
[4] takagi@nuem.nagoya-u.ac.jp

For finding the suspension geometry that reduces the road noise, the sensitivity analysis (1) with respect to the suspension connection points is presented in this paper. As an objective function, the input power to the vehicle is used from the fact that the statistical space averaged compartment cavity SPL is proportional to the input power from the point of view of power balance (2). In order to make the sensitivity analysis easy, the suspension arms are modeled as a rigid link whereas the body, the tire and the shock absorber are modeled as a modal model. The suspension geometry that reduces the input power is obtained by the shape optimization based on the sensitivities. Then, it is presented that the rigid links modeling is suitable for the design of the suspension geometry at the early stage of the vehicle development by investigating the characteristic of the suspension vibration behavior.

2. MODELING

The mechanism of structure born road noise can be thought as followings. First, the tires are excited by the forced displacement due to the roughness of the road surface. Then, the vibrations transmit to the vehicle body through the suspension subsystems. The each input power from the road surface to each tires is statistically uncorrelated. Therefore, the input power from the each tire can be considered separately. In this paper, the road noise from rear left side multi-link suspension is considered.

On the typical bending rigidity of the suspension arms and stiffness of the bushes, the arms behave like a rigid body in many of the multi-link suspension subsystem vibration mode shapes of which the natural frequencies are around frequencies of interest (e.g. around 150 Hz). Therefore, in order to make the investigation about the reduction of the road noise due to the configuration of suspension easy, the suspension model is simplified as rigid links connected with bushes. On the other hand, the vehicle body, the absorber and the tire subsystems have deformed vibration mode shapes at the frequencies of interest so that these are modeled as modal model which are identified either numerically or experimentally. The schematic of the modeling is shown in Fig. 1.

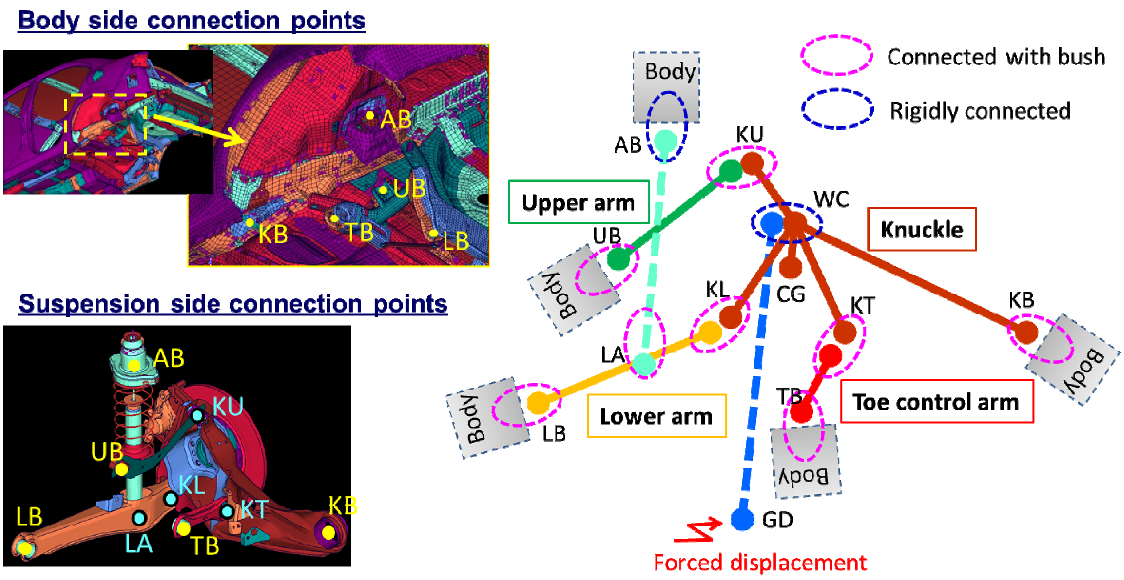

Figure 1 – schematic of proposed modeling

The suspension arm consists of the four rigid components which are knuckle, lower arm, upper arm and toe control arm as shown in Fig. 1. The rigid components are connected with bushes at points named KL, KU and KT. Then, the suspension arms are connected to the vehicle body with bushes at four points which are named LB, UB, TB and KB. The absorber connects the lower arm and the vehicle body at point LA and AB, respectively. At the point AB, the absorber is rigidly connected to the vehicle body whereas it is connected to the lower arm with bush at the point LA. The position of the point LA is determined by internally dividing a section from the point LB to KL by 3:1. The tire is rigidly connected to the knuckle at a point named WC and excited by the forced displacement at a point named GD.

3. GOVERING EQUATIONS

3.1 Degree Of Freedom

3.1.1 Suspension

In one rigid component, coordinates are taken into account at the center of gravity and each connection points. For example, the knuckle rigid component has following displacement vector $\mathbf{u}_{kcl}$,

$$\mathbf{u}_{kcl} = \left\{ \mathbf{u}_{kclWC}^T \quad \mathbf{u}_{kclKL}^T \quad \mathbf{u}_{kclKU}^T \quad \mathbf{u}_{kclKT}^T \quad \mathbf{u}_{kclKB}^T \quad \mathbf{u}_{kclO}^T \right\}^T, \tag{1}$$

where $\mathbf{u}_{kclWC}$, $\mathbf{u}_{kclKL}$, $\mathbf{u}_{kclKU}$, $\mathbf{u}_{kclKT}$, $\mathbf{u}_{kclKB}$ and $\mathbf{u}_{kclO}$ are the displacement vectors at the point WC, KL, KU, KT, KB and the center of gravity of the knuckle component, respectively. Each displacement vectors at connection points and center of gravity has translation and rotation DOFs in Cartesian coordinate (i.e. $\{u \quad v \quad w \quad \theta_x \quad \theta_y \quad \theta_z\}^T$ for each point displacement vectors), so that the total number of DOF of knuckle component is 36. The displacement vector of the suspension subsystem $\mathbf{q}$ is expressed by the rigid components displacement vectors as

$$\mathbf{q} = \left\{ \mathbf{u}_{kcl}^T \quad \mathbf{u}_{lwr}^T \quad \mathbf{u}_{upr}^T \quad \mathbf{u}_{toe}^T \right\}^T, \tag{2}$$

where $\mathbf{u}_{lwr}$, $\mathbf{u}_{upr}$ and $\mathbf{u}_{toe}$ are the displacement vector of the lower arm component, the upper arm component and the toe control arm component, respectively, like that of the knuckle component expressed in Eqn. (1). For displacement vectors $\mathbf{u}_{lwr}$, $\mathbf{u}_{upr}$ and $\mathbf{u}_{toe}$, the coordinates are taken at center of gravities and both ends of each arms. In addition, the coordinate at the point LA is taken for the lower arm component. So, the total number of DOF of the suspension subsystem displacement vector $\mathbf{q}$ is 96. Equation (2) can be reduced to the displacement vector $\mathbf{q}_o$ represented only independent displacement vectors of the each rigid components due to the geometrical constraint of the rigid links as

$$\mathbf{q} = \boldsymbol{\beta}\mathbf{q}_o, \tag{3a}$$

$$\mathbf{q}_o = \left\{ \mathbf{u}_{kclWC}^T \quad \mathbf{u}_{lwrO}^T \quad \mathbf{u}_{uprO}^T \quad \mathbf{u}_{toeO}^T \right\}^T, \tag{3b}$$

where $\boldsymbol{\beta}$ is rigid element matrix that expresses the linearized geometrical constraint of the rigid links. Therefore, the rigid element matrix is the function of the geometry of the suspension subsystem. In this paper, the displacement vectors at the point WC and center of gravities of the lower arm, upper arm and toe control arm are taken as independent displacement vectors. The number of DOF of independent displacement vector $\mathbf{q}_o$ is 24.

3.1.2 Vehicle body

The displacement vector of the vehicle body $\mathbf{u}_b$ is expressed by the modal coordinate in the global coordinate under the condition of being uncoupled with the suspension subsystem as

$$\mathbf{u}_b = \boldsymbol{\varphi}_b \boldsymbol{\xi}_b, \tag{4}$$

where $\boldsymbol{\varphi}_b$ is the mode shape matrix of the vehicle body and $\boldsymbol{\xi}_b$ is the modal amplitude vector of the vehicle body.

3.1.3 Tire

As well as the case of the vehicle body, the displacement vector of the tire $\mathbf{u}_t$ is also expressed by the modal coordinate in the global coordinate under uncoupled condition as

$$\mathbf{u}_t = \boldsymbol{\varphi}_t \boldsymbol{\xi}_t, \tag{5}$$

where $\boldsymbol{\varphi}_t$ is the mode shape matrix of the tire and $\boldsymbol{\xi}_t$ is the modal amplitude vector of the tire.

3.1.4 Absorber

The configuration of the absorber depends on that of the lower arm component so that the modal coordinate of the absorber has to be expressed in the local coordinate and is transformed to the global coordinate by the transformation matrix as

$$\mathbf{u}_a = \mathbf{T}_a \boldsymbol{\varphi}_a^{(l)} \boldsymbol{\xi}_a , \tag{6}$$

where $\mathbf{u}_a$ is the displacement vector of the absorber in the global coordinate and $\mathbf{T}_a$ is the transformation matrix from the local coordinate to the global coordinate. $\boldsymbol{\varphi}_a^{(l)}$ is the mode shape matrix of the absorber in the local coordinate, where the superscript (l) denotes that the mode shape matrix is described in the local coordinate. $\boldsymbol{\xi}_a$ is the modal amplitude vector of the absorber.

3.2 Couplings

The coupling with the bush is described as the force to the coupled subsystem. For example, the coupling force between the vehicle body and the lower arm at point LB is described as

$$\mathbf{f}_{bLB} = -\mathbf{f}_{lwrLB} = -\mathbf{K}_{LB}^{(g)} \left(\mathbf{u}_{bLB} - \mathbf{u}_{lwrLB} \right), \tag{7}$$

where $\mathbf{f}_{bLB}$ and $\mathbf{f}_{lwrLB}$ are the force to the vehicle body and to the lower arm at the point LB, respectively. $\mathbf{K}_{LB}^{(g)}$ is the stiffness matrix of the bush at the point LB. The superscript (g) denotes that the stiffness matrix is expressed in the global coordinate. $\mathbf{u}_{bLB}$ and $\mathbf{u}_{lwrLB}$ are the displacement vector of the vehicle body and the lower arm at the point LB, respectively.

The rigid connected displacement couplings are considered by constraint equations. The constraint equations of the system are followings.

$$\mathbf{u}_{bAB} - \mathbf{u}_{aAB} = \mathbf{0} . \tag{8a}$$

$$\mathbf{u}_{tWC} - \mathbf{u}_{kclWC} = \mathbf{0} . \tag{8b}$$

$$v_{tGD} = 1 . \tag{8c}$$

Equations (8a) and (8b) are the rigid connection coupling at the point AB and WC respectively. Equation (8c) is the constraint equation at the point GD, which describes the forced displacement input. In this paper, the focus is on the input power around 150 Hz. In such frequencies, it is known that the contribution from the y directional forced displacement v_{tGD} has high contribution to the road noise so that unit y directional displacement at the point GD is considered as input.

3.3 Equation of Motion

The equation of motion of the system can be written considering the couplings at all the connection points as

$$\begin{bmatrix} \mathbf{D}_b & & & & sym. \\ \mathbf{0} & \mathbf{D}_a & & & \\ \mathbf{0} & \mathbf{0} & \mathbf{D}_t & & \\ \mathbf{C}_{qb} & \mathbf{C}_{qa} & \mathbf{0} & \mathbf{D}_q & \\ \mathbf{C}_{cb} & \mathbf{C}_{ca} & \mathbf{C}_{ct} & \mathbf{C}_{cq} & \mathbf{0} \end{bmatrix} \begin{Bmatrix} \boldsymbol{\xi}_b \\ \boldsymbol{\xi}_a \\ \boldsymbol{\xi}_t \\ \mathbf{q} \\ \boldsymbol{\lambda} \end{Bmatrix} = \begin{Bmatrix} \mathbf{0} \\ \mathbf{0} \\ \mathbf{0} \\ \mathbf{0} \\ \mathbf{u}_0 \end{Bmatrix}, \tag{9}$$

where $\mathbf{D}_b$, $\mathbf{D}_a$, $\mathbf{D}_t$ and $\mathbf{D}_q$ are the dynamic stiffness matrixes of the each subsystems which take into account the stiffness of the bushes at the connection points. $\mathbf{C}_{qb}$ and $\mathbf{C}_{qa}$ are the coupling matrixes due to the bushes between the suspension and the vehicle body, the suspension and the absorber, respectively. $\mathbf{C}_{cb}$, $\mathbf{C}_{ca}$, $\mathbf{C}_{ct}$ and $\mathbf{C}_{cq}$ are the Jacobian matrixes of the constraint equations and $\boldsymbol{\lambda}$ is the Lagrange multiplier. $\mathbf{u}_0$ is the input vector due to the forced displacement of

Eqn. (8c). By considering the rigid link relation of Eqn. (3a), the equation of motion of the system can be finally obtained as

$$\mathbf{D}\mathbf{x} = \mathbf{F}\,. \tag{10a}$$

$$\mathbf{D} = \begin{bmatrix} \mathbf{D}_b & & & sym. & \\ \mathbf{0} & \mathbf{D}_a & & & \\ \mathbf{0} & \mathbf{0} & \mathbf{D}_t & & \\ \boldsymbol{\beta}^T\mathbf{C}_{qb} & \boldsymbol{\beta}^T\mathbf{C}_{qa} & \mathbf{0} & \boldsymbol{\beta}^T\mathbf{D}_q\boldsymbol{\beta} & \\ \mathbf{C}_{cb} & \mathbf{C}_{ca} & \mathbf{C}_{ct} & \mathbf{C}_{cq}\boldsymbol{\beta} & \mathbf{0} \end{bmatrix},\quad \mathbf{x} = \begin{Bmatrix} \boldsymbol{\xi}_b \\ \boldsymbol{\xi}_a \\ \boldsymbol{\xi}_t \\ \mathbf{q}_o \\ \boldsymbol{\lambda} \end{Bmatrix},\quad \mathbf{F} = \begin{Bmatrix} \mathbf{0} \\ \mathbf{0} \\ \mathbf{0} \\ \mathbf{0} \\ \mathbf{u}_0 \end{Bmatrix} \tag{10b}$$

3.4 Input Power to the Body

The Input power to the vehicle body Π is expressed by the summation of the input powers at the each connection points as

$$\Pi = \Pi^{LB} + \Pi^{UB} + \Pi^{TB} + \Pi^{KB} + \Pi^{AB}\,, \tag{11}$$

where the superscript denotes the connection point from which the input power is supplied. As an example, the input power from the connection point LB is written as

$$\Pi^{LB} = \frac{-j\omega}{2}\mathbf{f}_{bLB}\cdot\mathbf{u}^*_{bLB}\,. \tag{12}$$

The superscript * denotes complex conjugate and ω is angular frequency. Substituting Eqns. (2), (4) and (7) into Eqn. (12), Π^{LB} can be expressed in a function of $\boldsymbol{\xi}_b$ and $\mathbf{q}$. For the connection point UB, TB and KB, the input power at the connection point can be obtained in the same manner as the point LB. The input power from the point AB can be expressed in the modal coordinate of the vehicle body as

$$\Pi^{AB} = \frac{-j\omega}{2}\mathbf{f}_{bAB}\cdot\mathbf{u}^*_{bAB} = \frac{j\omega}{2}\left(\mathbf{C}^T_{cb}\boldsymbol{\lambda}\right)\cdot\boldsymbol{\xi}^*_b\,. \tag{13}$$

In the expansion of Eqn. (13), it is used that the constraint force at the connection point AB can be expressed using the Lagrange multiplier as $-\mathbf{C}^T_{cb}\boldsymbol{\lambda}$. Substituting Eqns. (12) and (13) into Eqn. (11), and taking into account the first equation of Eqn. (9), the total active input power to the vehicle body is expressed as follows.

$$\mathrm{Re}\{\Pi\} = \frac{1}{2}\boldsymbol{\xi}^H_b\mathbf{R}\boldsymbol{\xi}_b\,, \tag{14a}$$

$$R_{ij} = \begin{cases} \omega^2\omega_{bi}\eta_{bi}, & (i=j) \\ 0, & (i\neq j) \end{cases}, \tag{14b}$$

where the superscript H denotes conjugate transpose. ω_{bi} and η_{bi} are the natural angular frequency and the modal damping loss factor of the i th vehicle body mode, respectively. The form of Eqn. (14) is equal to the dissipation power within the vehicle body subsystem. This indicates the equality of the input power and the dissipation power, so called power balance.

3.5 Sensitivity Analysis

For finding the suspension geometry which reduces the input power to the vehicle body, the sensitivity analysis with respect to the position of the connection point is used. The position of the point KL, KU and KT are taken as design variable γ in this paper. From the fact that the matrix $\mathbf{R}$ in Eqn. (14) is not a function of design variable γ, the sensitivity can be written as

$$\frac{\partial \operatorname{Re}\{\Pi\}}{\partial \gamma} = \operatorname{Re}\left\{\frac{\partial \boldsymbol{\xi}_b^H}{\partial \gamma} \mathbf{R} \boldsymbol{\xi}_b\right\}. \tag{15}$$

From Eqn. (10b), $\boldsymbol{\xi}_b$ is part of $\mathbf{x}$ so that $\partial \boldsymbol{\xi}_b / \partial \gamma$ can be obtained from $\partial \mathbf{x} / \partial \gamma$. First order sensitivity of $\mathbf{x}$ can be lead from Eqn. (10a) by considering that $\mathbf{F}$ is not a function of design variable,

$$\frac{\partial \mathbf{x}}{\partial \gamma} = -\mathbf{D}^{-1} \frac{\partial \mathbf{D}}{\partial \gamma} \mathbf{x}. \tag{16}$$

The derivative $\partial \mathbf{D} / \partial \gamma$ can be calculated algebraically or numerically.

4. RESULTS

4.1 Validity of Modeling

For the proposed rigid arm modeling, the concentrated masses of the each rigid components are estimated from the detail 3D geometry. For the knuckle rigid component, the masses of the brake rotor and the caliper are considered in addition to that of the knuckle arms. In Fig. 2, the comparison of the input power between the detail FE model and the proposed rigid arm modeling is shown. Less difference can be seen between the two modeling especially around frequencies of large input power (e.g. from 100 Hz to 200 Hz). This indicates that the influence of the bending rigidities of the arms can be neglected to describe the vibration behavior of the system at the frequencies of interest.

The shapes of the suspension arms are neither straight nor uniform cross section. However, for the simplified case, it is considered that the arms are assumed to have the center of gravity at the geometrical center (i.e. the arm shapes are assumed to be straight beam with uniform cross section). There is also less difference between the simplified and the exact case. This indicates that the detail mass distribution could not be important unless the drastic mass distribution is considered. In other word, the road noise could be predicted without the detail information of the arm shapes. This characteristic can make application of the modeling possible at the early stage of the vehicle development in which the detail arm shapes are not decided.

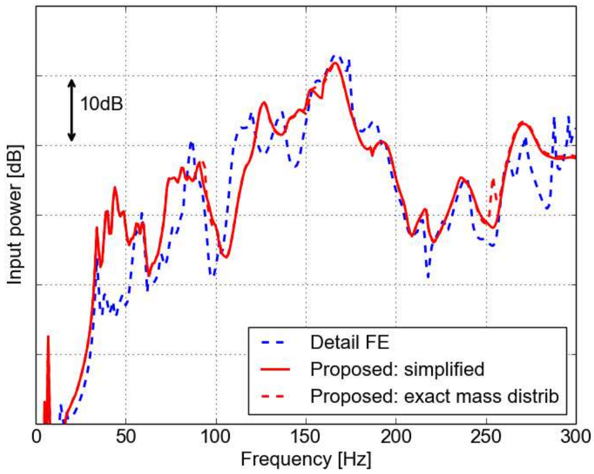

Figure 2 – Validity of the proposed rigid arm suspension modeling. Input power computed from detail FE model (blue dashed), from the proposed simplified rigid arm modeling (red solid), from the proposed rigid arm modeling with exact mass distribution property (red dashed).

4.2 Sensitivity Analysis

By the rigid arm suspension modeling, the sensitivity analysis can be conducted using Eqns. (15) and (16). The x, y, z positions of the point KL, KU and KT are taken as design variables (i.e. totally nine design variables), and the overall of input power from 100 Hz to 200 Hz is taken as an objective function.

With the design variables taken in this paper, the derivative $\partial \mathbf{D}/\partial\gamma$ of Eqn. (16) is able to be evaluated without uncertainty, except the part of the derivative of the mass matrix of the suspension subsystem. The derivatives of the mass matrix of the suspension subsystem is expressed as

$$\frac{\partial \mathbf{M}_q^{(g)}}{\partial\gamma} = \frac{\partial \mathbf{T}}{\partial\gamma}\mathbf{M}_q^{(l)}\mathbf{T}^T + \mathbf{T}\frac{\partial \mathbf{M}_q^{(l)}}{\partial\gamma}\mathbf{T}^T + \mathbf{T}\mathbf{M}_q^{(l)}\frac{\partial \mathbf{T}^T}{\partial\gamma}. \quad (17)$$

where $\mathbf{M}_q^{(g)}$, $\mathbf{M}_q^{(l)}$ are mass matrixes of suspension subsystem. The superscript denotes the coordinate in which the mass matrix is expressed. $\mathbf{T}$ is transformation matrix from local coordinate to global. On the right hand side of Eqn. (17), the first and the third terms describe the contribution from geometrical change with constant mass properties, while the second term describes the contribution from the mass change of the rigid arms themselves due to their length changes. In general, the shapes of the suspension arm components can be arbitrary (e.g. an arm with tapered cross section, a curved arm and so on). Therefore, the derivatives of the mass matrixes of the second term of Eqn. (17) cannot be determined uniquely. In order to calculate the derivatives, one nominal arm shape is considered that the arm has straight with uniform cross section assumed as simplified case in the rigid arm modeling of Sec. 4.1. For calculating the derivatives of the knuckle component mass matrix, it is assumed that the mass increases proportional to knuckle arm length extension at the connection point. The increase rate is estimated as 4 kg per unit length from the actual mass distribution of the knuckle.

The sensitivity results are shown in Fig. 3 with the both cases in which the derivatives of the mass matrixes are taken into account or not. The negative sensitivity shown in Fig. 3 means that the input power is increased with the negative direction position change (e.g. replacing z coordinate of the point KL along -z axis increases input power).

In Fig. 3, less difference can be seen between the both cases either with or without the consideration of the mass matrixes derivatives. This indicates that the mass property changes could not be important. This characteristic is also convenient for the application at the early stage of vehicle development.

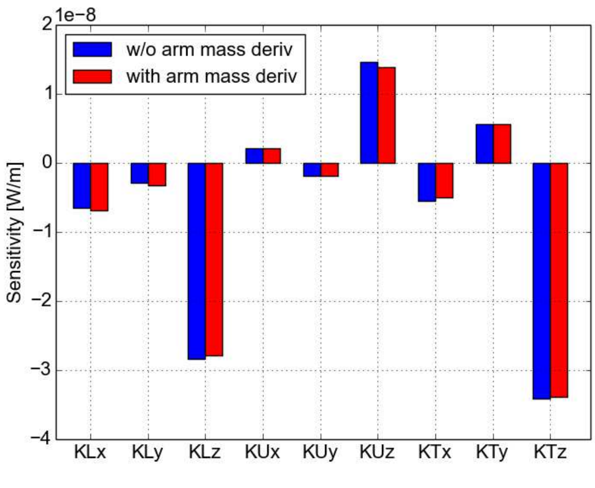

Figure 3 – Input power sensitivity with respect to the positions of the connection points KL, KU and KT.
The derivatives of the arms masses are not taken into account (blue), are taken into account (red).

4.3 Shape Optimization

4.3.1 Optimized results

Using the sensitivity analysis, a shape optimization can be conducted. From the result of Sec. 4.1 and 4.2, the arms are simplified as straight with uniform cross section and the mass matrixes derivatives are neglected in the sensitivity analysis. Besides, the mass properties of the arms on their principal axes are kept constant during the optimization process (i.e. each rigid components respectively has the same mass property as the initial shapes on their local principal axes, but the influences due to the geometrical transformations are taken into account). The flowchart of the optimization is shown in Fig. 4. MMA (3) was used as an optimization method.

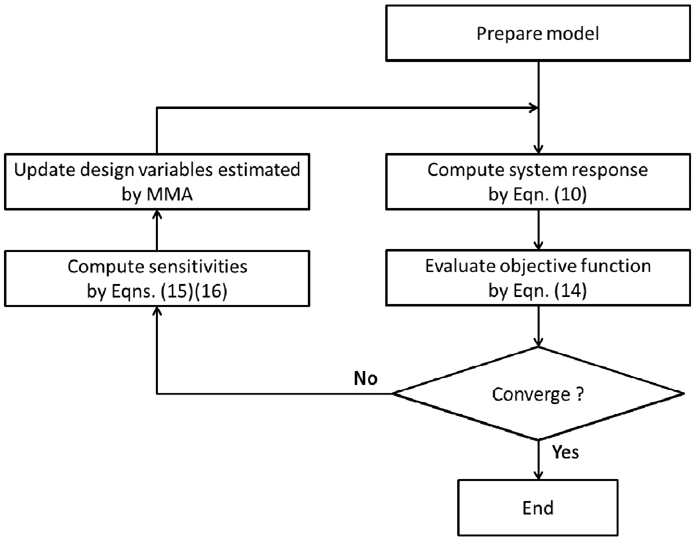

Figure 4 – Flowchart of the optimization

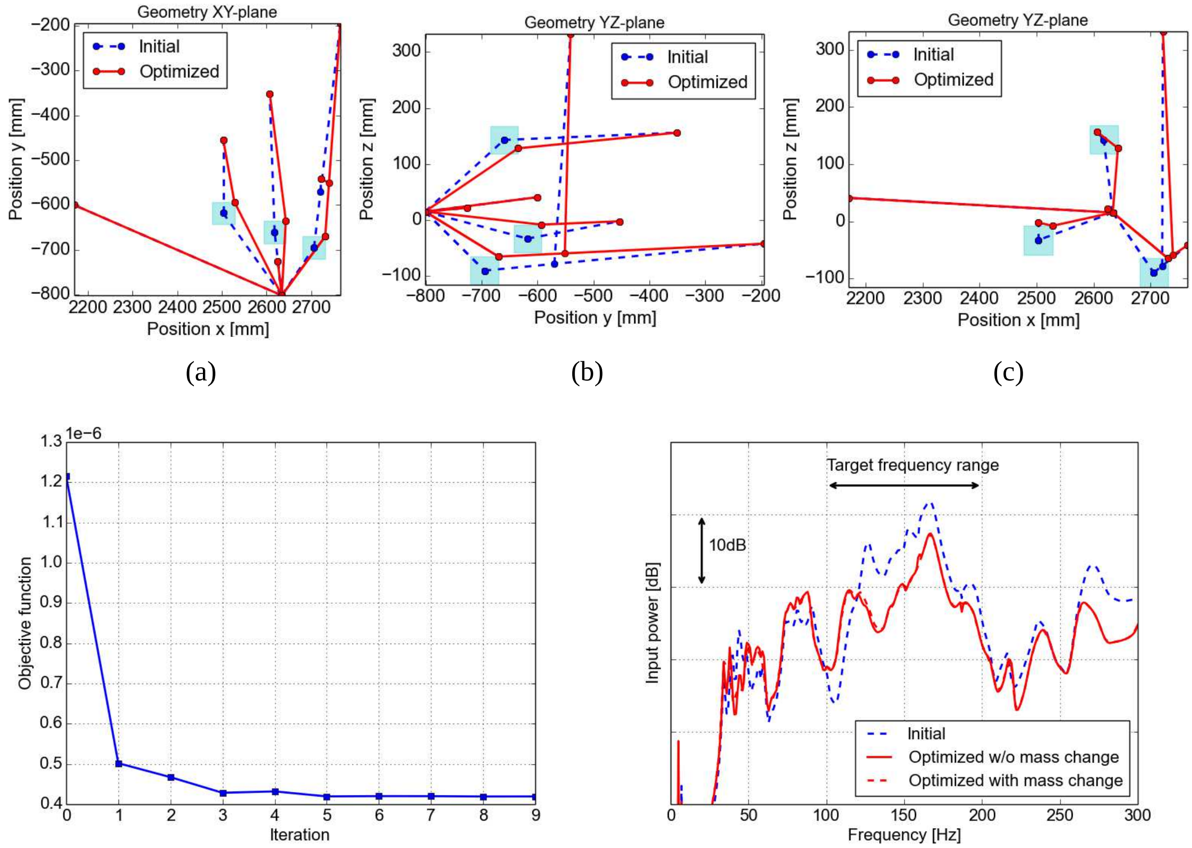

Figure 5 – The optimization results: (a) (b) (c) Comparison of the geometry in each plane views between the initial (blue dashed) and the optimized (red solid). The design spaces are shown in cyan patch. (d) The optimization history. (e) Comparison of the input power between the initial (blue dashed), the optimized without mass change (red solid) and the optimized with mass change (red dashed).

The optimization results are shown in Fig. 5. The design spaces were taken -25 mm to 25mm from the point KL, KU and KT initial positions for all directions, which are shown in Figs. 5(a)-(c) as cyan square patch. It is observed that the optimization is well converged from the optimization history of Fig. 5(d). In Fig. 5(e), it can be found that the input power is reduced in the frequencies of optimization target. The influence of the mass changes due to the arm length changes is also investigated. The input power that considers the mass changes at the optimization configuration is also plotted in Fig. 5(e). The mass change of the rigid arms is calculated from the assumption used in Sec. 4.2. The two spectra are almost the same so that it is confirmed that the assumption of keeping the mass properties of the rigid components constant is valid.

4.3.2 **Input power contribution**

The optimization results can be diagnosed by the input power contribution. The input power contributions from the each connection points are plotted in Fig. 6 for the initial configuration and the optimized. Figures 6(a) and 6(b) show the magnitude of the input power whereas Figs. 6(c) and 6(d) show the positive/negative contribution by the normalized input power expressed in the following equation. As an example, the normalized input power from the point LB Π_{nor}^{LB} is written as

$$\Pi_{nor}^{LB} = \Pi^{LB} / \left(\left|\Pi^{LB}\right| + \left|\Pi^{UB}\right| + \left|\Pi^{TB}\right| + \left|\Pi^{KB}\right| + \left|\Pi^{AB}\right| \right). \tag{18}$$

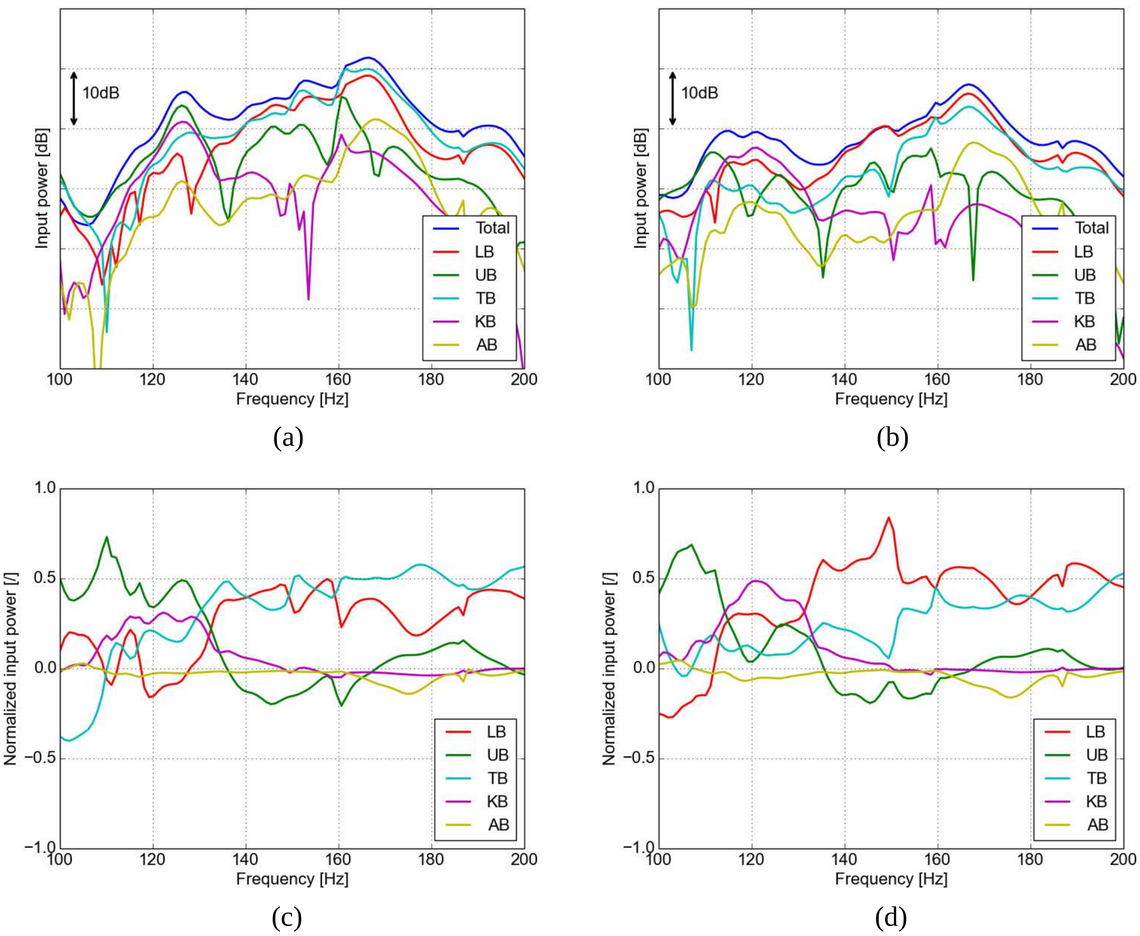

Figure 6 – Input power from each connection points: (a) Input power in the case of the initial in dB scale. (b) Input power in the case of the optimized in dB scale. (c) Normalized input power in the case of the initial. (d) Normalized input power in the case of the optimized.

The negative normalized input power means that the energy of the vehicle body is dissipated by the excitation at the connection point due to the opposite direction of the force and the vibration. The normalized input power can be used as the indicator for understanding the mechanism of the input power reduction. The decrease of positive normalized input power means that the input power reduction could be achieved by the reduction of vibration velocity of the rigid arm itself whereas the increase of the negative input power contribution means that the input power reduction could be achieved by cancelation among the input power from each connection points.

From Figs. 6(a) and 6(b), the reduction of the input power over entire frequencies is mostly achieved by reducing the contribution from the point TB. Around 125 Hz, the input power reduction from the point UB also contributes to the input power reduction. In Figs. 6(c) and 6(d), the signs and the negative contribution of the normalized input power have same tendency between the initial and the optimized over entire frequencies (except around 125 Hz). This indicates that the input power reduction could be achieved by the reducing the vibration of the highly contributed rigid suspension arm without increasing the vibration of the other arms.

5. DISCUSSION

The optimized suspension geometry shown in Figs. 5(a)-(c) may not achieve the compatibility between NVH and handling stability at high quality (e.g. camber compliance might be increased due to the small z directional width). In order to achieve the purpose, limitations about handling stability should be considered in the optimization process. If an optimal result doesn’t reduce the input power enough by taking into account the limitations, adding the stiffness of the bushes to the design variables might improve the results (in such case, considering weigh function for the sensitivities would be necessary because of the difference in sensitivity unit between the arm connection position and stiffness of bush).

6. CONCLUSIONS

The sensitivity analysis with respected to the connection positions was conducted by modeling the suspension as rigid arms. The modeling was validated by comparing the input power with that calculated by the detail FE model. The optimized suspension geometry that minimizes the input power was calculated using the shape optimization based on the sensitivity analysis. In the sensitivity analysis and the shape optimization, it was found that the influence of the mass changes was not important for the input power compared to that of geometrical change. Therefore the suspension arms could be modeled as straight with uniform cross section rigid beam. This characteristic is suitable for the application at the early stage of the vehicle development in which the suspension geometry can be only modified.

REFERENCES

1. Haug EJ, Choi KK, Komkov V. Design sensitivity analysis of structural systems. Academic Press, Inc.; 1986.
2. Kadomatsu K, Iwanaga Y. Vibro-acoustic transfer function and driving-point conductance for vehicle body. Transactions of the Japan Society of Mechanical Engineering. 2002; 68(672):3561-3565
3. Krister S. The method of moving asymptotes - a new method for structural optimization. International Journal for Numerical Methods in Engineering. 1987; 24:359-373